Desalination and Water Treatment
www.deswater.com
doi: 10.5004/dwt.2019.24122

162 (2019) 207–219
September

Simultaneous adsorptive removal of organic and inorganic pollutants from aqueous solutions: kinetic, equilibrium and thermodynamic studies

Reza Saeedi[a], Shahla Mozaffari[b], Elham Beigi[b], Shokooh Sadat Khaloo[a,*]

[a]*Department of Health, Safety and Environment (HSE), School of Public Health and Safety, Shahid Beheshti University of Medical Sciences, Tehran, Iran, Tel. +98-21-22432043; Fax: +98-21-22432036; email: sh_khaloo@sbmu.ac.ir (S.S. Khaloo), Tel. +98-21-22432040-41; Fax: +98-21-22432037; email: reza.saeedi@gmail.com (R. Saeedi)*
[b]*Department of Chemistry, Payame Noor University, Tehran, Iran, Tel. +98-2186010183-4; emails: mozaffari766@yahoo.com (S. Mazaffari), beigielham@yahoo.com (E. Beigi)*

Received 1 September 2018; Accepted 14 March 2019

ABSTRACT

There is an increasing need for clean water to support human societies and other living organisms. Ferrite-based magnetic nano-materials are an important class of metal oxide composite with unique physicochemical properties which make them as a powerful candidate for water purification. In this study, $MnFe_2O_4$-graphene oxide nano-composite (MNC) was synthesized and characterized by scanning electron microscopy, energy dispersive spectroscopy, thermogravimetric analysis, vibrating sample magnetometer and X-ray diffraction techniques. MNC was used for adsorptive removal of organic (Methylene Blue, Toluidine Blue) and inorganic (Co and Ni) pollutants, simultaneously. The adsorptive removal efficiency of MNC for organic and inorganic pollutants was optimized with respect to different factors such as pH, contact time, adsorbent dose, the initial pollutant concentration and temperature. The results of the adsorption process were well fitted with the Langmuir isotherm and pseudo-second-order kinetic model (R^2 > 0.99). The maximum adsorption capacity according to the Langmuir isotherm model (q_m) was 37.0, 46.7, 125.0 and 110.0 mg g^{-1} for Co(II), Ni(II), MB and TB, respectively. The negative values of $\Delta G°$ (–25.1 to –31.1 kJ mol^{-1}) and positive values of $\Delta H°$ (46.8–118.7 kJ mol^{-1}) suggested that the adsorption process is spontaneous and endothermic. The adsorption capacities of MNC in five cycles of consecutive adsorption–desorption experiments approved that the sorbent could keep 97% of the capability in adsorptive removal of the mentioned pollutants then the prepared MNC was introduced as a highly efficient multifunctional, magnetically separable and reusable adsorbent for water remediation.

Keywords: Cobalt; Magnetic graphene; Methylene Blue; Toluidine Blue; Removal

1. Introduction

As industrialization and scientific improvements have spread around the world, the problem of pollution especially water pollution has spread with them. Population growth, climate change, increasing water scarcity and urbanization already pose challenges for water supply systems. According to the WHO fact sheets by 2025, half of the world's population will be living in water-stressed areas [1]. The intelligent use and maintenance of water supplies are the most important challenges that stand before mankind. Organic compounds and heavy metal ions are the most concerning pollutants in water. The best option for managing the waste which cannot be eliminated at the source includes recycling, refining, or recovering the waste for reuse [2]. Various techniques of water treatment have been used including electro-flocculation [3], oxidation [4], photo-catalytic degradation [5] and adsorption [6–9]. Among them, adsorption is one of the most commonly applied techniques. To date, different kinds of materials have been applied as high-performance adsorbents such as

* Corresponding author.

carbon-based nano-materials. Graphene, two-dimensional sheets of carbon atoms with sp^2 hybridization arranged in the form of a honeycomb lattice, developed as a member of carbon materials. It has earned the title "miracle material" due to its excellent electrical and mechanical properties, high thermal conductivity and extraordinary quantum Hall effects. Graphene has attracted great attention since it is discovered in 2004 [10]. Currently, graphene has become one of the most prominent nano-scale materials and has various applications in many fields such as super-capacitors [11], quantum dots [12], sensors [13,14] and energy storage [15,16]. Some new applications have been developed with the modification of graphene and graphene oxide. Decorating other nano-materials [17,18] and grafting functional groups [19,20] onto graphene nano-sheets and doping other atoms in the crystal lattice of graphene nano-sheets [21,22] have been developed and have widened the application fields of graphene. In recent years, a great deal of attention has been paid for application of graphene and its derivative in environmental remediation and wastewater treatment. Although graphene has impressive adsorption capacities towards various chemicals, the very small particle size of graphene and graphene oxide can cause the serious problem in its application in a batch and fixed-bed column systems. These problems could be overcome by covalently bonding nano-sorbent on suitable supports [23] or by the decoration of magnetic nanoparticles onto graphene nano-sheets [24,25]. Magnetic carrier technology, first reported by Robinson et al. [26] in 1973, can avoid tedious steps of centrifugation or filtration in the water remediation process. Many studies have reported the preparation of magnetic graphene. Chong et.al. [4] synthesized magnetic Fe^0/Fe_3O_4/graphene by a one-step reduction method and investigated its application in rapid degradation of dyes such as Methyl Orange, Methylene Blue and Crystal Violet [4]. Hoan et al. [27] reported a synthesis of reduced graphene oxide modified by magnetic iron oxide and its application for As(V), Ni(II) and Pb(II) removal. Moradi [28] reported a magnetic graphene oxide as a high-performance adsorbent for amoxicillin removal from water in 2015. Ting et al. [29] in 2016 synthesized magnetic graphene/Fe_3O_4 composite by via graphene oxide oxidizing $FeCl_2$ in situ and applied to remove Pb(II), Cu(II) and Zn(II) with an efficiency of almost 100%.

In this study, $MnFe_2O_4$-GO magnetic nano-composite (MNC) was synthesized and applied for co-removal of the organic and inorganic pollutants from the water. MNC was synthesized using hydrothermal co-precipitation method and its structure was characterized using scanning electron microscopy (SEM), energy dispersive X-ray spectroscopy (EDS) and X-ray powder diffraction (XRD). The adsorptive behaviour of MNC was investigated in the removal of Co(II), Ni(II) as candidates of heavy metal ions and Methylene Blue and Toluidine Blue as candidates of organic pollutant. The adsorption, kinetic and thermodynamic parameters of adsorption process as well as recycling of sorbent were investigated.

2. Materials and methods

2.1. Chemicals and reagent

$FeCl_3.6H_2O$, $MnCl_2.4H_2O$, potassium permanganate, graphite powder, sulfuric acid (95%), hydrogen peroxide (30%, w/w), sodium bisulfate, Methylene Blue, Toluidine Blue and standard solution of Co(II) and Ni(II) (1,000 mg L^{-1}) were purchased from Merck (Darmstadt, Germany). All chemicals were of analytical grade and used as received without further purification. De-ionized water (DI) was used as the solvent throughout the experiments. All of the working solutions used for optimization and establishing the isotherms were prepared by successive dilution of stock solutions. All the experiments were replicated two times and the average values were reported as the results.

2.2. Synthesis of $MnFe_2O_4$-graphene oxide

Graphene oxide (GO) was synthesized from graphite powder by the modified Hummers' method according to our previous report [23]. The magnetic nano-composite of $MnFe_2O_4$-graphene oxide was prepared in one-step hydrothermal method. In a typical procedure, the as-prepared graphene oxide (300 mg) was exfoliated by sonication in 50 mL of DI for 20 min. After that, 30 mL aqueous solution containing 1 g of $FeCl_3.6H_2O$ and 0.376 g of $MnCl_2.4H_2O$ (molar ratio of Fe: Mn, 2:1) was added to the GO suspension at 70°C followed by stirring for 20 min. After that, pH of the mixture was adjusted to 11 by adding NaOH solution 1 M dropwise. The mixture was then transferred into a 100 mL Teflon-lined stainless steel autoclave and heated at 200°C for 12 h. A solid black product was obtained and was washed several times with de-ionized water and dried in an oven at 60°C overnight.

2.3. Adsorption experiments

2.3.1. Effect of experimental parameters on adsorption of organic or inorganic pollutant in a single system

In the present study, a batch mode operation at room temperature was selected in order to evaluate the adsorption process of an organic or inorganic pollutant on MNC. The effect of pH (4–8), contact time (3–60 min) and adsorbent dose (0.4–1.1 g L^{-1}) on adsorptive removal efficiency of MNC were studied. In a typical experiment, a certain amount of nano-composite and 100 mL solution with varying concentrations (10–100 mg L^{-1}) of organic or inorganic contaminant were mixed together and stirred on a shaker at 500 rpm. 5.0 mL solution of inorganic samples or 1.0 mL of organic samples were taken at given time intervals and the solids were removed by a magnet. The temporal concentration of the organic pollutants in the supernatant was analyzed by a UV–Vis spectrophotometer (AvaSpec-2048, Avantes, Netherlands) and concentrations of inorganic pollutants were determined by an inductively coupled plasma optical emission spectrometer (ICP OES, Varian 710 ES, Victoria, Australia). Adsorption capacities of MNC (q_t, mg g^{-1}) for each pollutant were calculated on the basis of the following equation:

$$q_t = \frac{C_0 - C_t}{m} \times V \tag{1}$$

where q_t is the temporal loading of adsorbate on sorbent (mg g^{-1}), C_0 and C_t are the initial and residual concentration

of adsorbate in solution (mg L^{-1}) at time t, respectively. V is the volume of the solution (L) and m is the mass of sorbent, MNC (g).

2.3.2. Adsorption kinetic study

In order to predict the adsorption kinetics of each pollutant on the MNC, experiments were conducted at pH 7.0, adsorbent dose (0.8 g L^{-1}) and pollutant concentration 30 mg L^{-1} at room temperature. The obtained data were analyzed using pseudo-first-order and pseudo-second-order models (Eqs. (2) and (3)) to investigate the mechanism of sorption [30].

$$\log\left(q_e - q_t\right) = \log q_e - \frac{k_1}{2.303}t \tag{2}$$

$$\frac{t}{q_t} = \frac{1}{q_e}t + \frac{1}{k_2 q_e^2} \tag{3}$$

where q_e and q_t (mg g^{-1}) are the adsorption capacities at equilibrium and time t (min), respectively. k_1 (min^{-1}) is the rate constant in the pseudo-first-order adsorption process. It is obvious the constant k_1 could be determined experimentally by plotting of $\log(q_e - q_t)$ vs. t. k_2 (g mg^{-1} min^{-1}) is the second ordered rate constant of adsorption. By plotting a curve of t/q_t against t, the parameters of q_e and k_2 could be evaluated.

2.3.3. Adsorption equilibrium study

After the optimization of the removal process, adsorption isotherm studies were conducted at room temperature with the constant amount of sorbent (0.8 g L^{-1}) to evaluate the efficiency of the adsorbent for the removal of the pollutants. After the introduction of the sorbent to the solution containing the contaminants with the initial concentration range of 10–100 mg L^{-1}, samples were stirred for 20 min, removal of nano-adsorbent from the reaction mixtures was carried out by an external magnet and the residual concentration of inorganic or organic pollutant was analyzed by ICP OES or UV–Vis spectrophotometers, respectively. For modelling of the adsorption process, two adsorption models were used: Langmuir and Freundlich models, Eqs. (4) and (5), respectively.

Original form:

$$q_e = \frac{bq_m C_e}{1 + bC_e} \tag{4}$$

$$\log q_e = \log K_f - \frac{1}{n}\log C_e \tag{5}$$

where C_e is the equilibrium concentration of adsorbate in solution (mg L^{-1}), q_e is the equilibrium loading of adsorbate on sorbent (mg g^{-1}), q_m and b are the Langmuir constants related to maximum adsorption capacity (mg g^{-1}), and the relative energy of adsorption (L mg^{-1}), respectively. K_f and n are the Freundlich constants related to adsorption capacity and adsorption intensity, respectively and the other parameters have the same meaning as mentioned earlier.

2.3.4. Adsorption study in multiple contaminant systems

In this set of experiments, at first the adsorption study in organic/inorganic binary systems was conducted and afterwards adsorption study in the presence of all four pollutants was done. The concentration of each pollutant is the same at 30 mg L^{-1} to study the competitive adsorption of pollutants and other coexistent ions on MNC.

2.3.5. Recovery experiments

To test the recoverability of MNC 20 mg of nano-composite was added to 25 mL of the solution containing 15 mg L^{-1} organic or inorganic pollutant and the mixture was shaken for 20 min. After separation of adsorbent from the solution by an external magnet, the equilibrium concentrations of organic or inorganic pollutants were measured while MNC was treated by shaking in 3 mL 0.01 M Na_2EDTA or 3 mL 0.1 M HCl for 10 min to recover the magnetic nano-composite in inorganic and organic treatment, respectively. The recovered MNC were reused for the next adsorption experiment to investigate the cyclic adsorption assay.

3. Results and discussion

3.1. Characterization of MNC

The $MnFe_2O_4$-GO nano-particles were characterized by SEM, (MIRA3, TESCAN, Czech Republic) equipped with EDS accessory and XRD (D8 Advanced diffractometer, Bruker, Germany) techniques. An overview of the morphology of GO and MNC has been shown in Fig. 1. The average thickness of the graphene oxide flake measured using SEM is ~2.1 nm and the particle size of $MnFe_2O_4$ is less than 20 nm. The elements on the surface of magnetic adsorbent were determined by EDS analysis (Fig. 1c). The EDS spectrum demonstrated the presence of C, O, Mn and Fe on the surface of MNC. C element comes from the graphene nano-sheets but O attributed to both graphene oxide and $MnFe_2O_4$ nano-particles and Si element is from the plated element for TEM measurement.

The XRD patterns of the GO, $MnFe_2O_4$ and $MnFe_2O_4$-GO are shown in Fig. 1d. A sharp diffraction peak at around $2\theta = 10.2°$ which correspond to (001) plane of GO and no obvious peak of graphite, indicates the formation of GO from graphite. As presented in Fig. 1d $MnFe_2O_4$ the characteristic peaks at $2\theta = 18.5°$, 30.9°, 35.6°, 38.9°, 44.6°, 55.8° and 64.4° can be indexed as the (111), (220), (311), (400), (422), (511) and (440) crystal planes of $MnFe_2O_4$, respectively. The XRD pattern of MNC is almost identical to that of the $MnFe_2O_4$ with the extra peak at around 10°, these results confirmed that the nano-particles of $MnFe_2O_4$ coated on GO and MNC composite were prepared successfully.

The vibrating sample magnetometer (VSM/AGFM, Meghnatis Daghigh Kavir Co., Iran) was used to study the magnetic property of $MnFe_2O_4$ and $MnFe_2O_4$-GO at room temperature (Fig. 2a). The maximum saturation magnetization of $MnFe_2O_4$-GO was measured at 20.99 (emu g^{-1}), which is lower than that of $MnFe_2O_4$ 30.15 (emu g^{-1}). The results showed that the addition of non-magnetic GO led to a decrease in the magnetic saturation of MNC but it was still strong enough for a convenient magnetic separation as shown in the inset of Fig. 2a. The black particles of $MnFe_2O_4$-GO attracted to the wall of the vial in the presence of an external

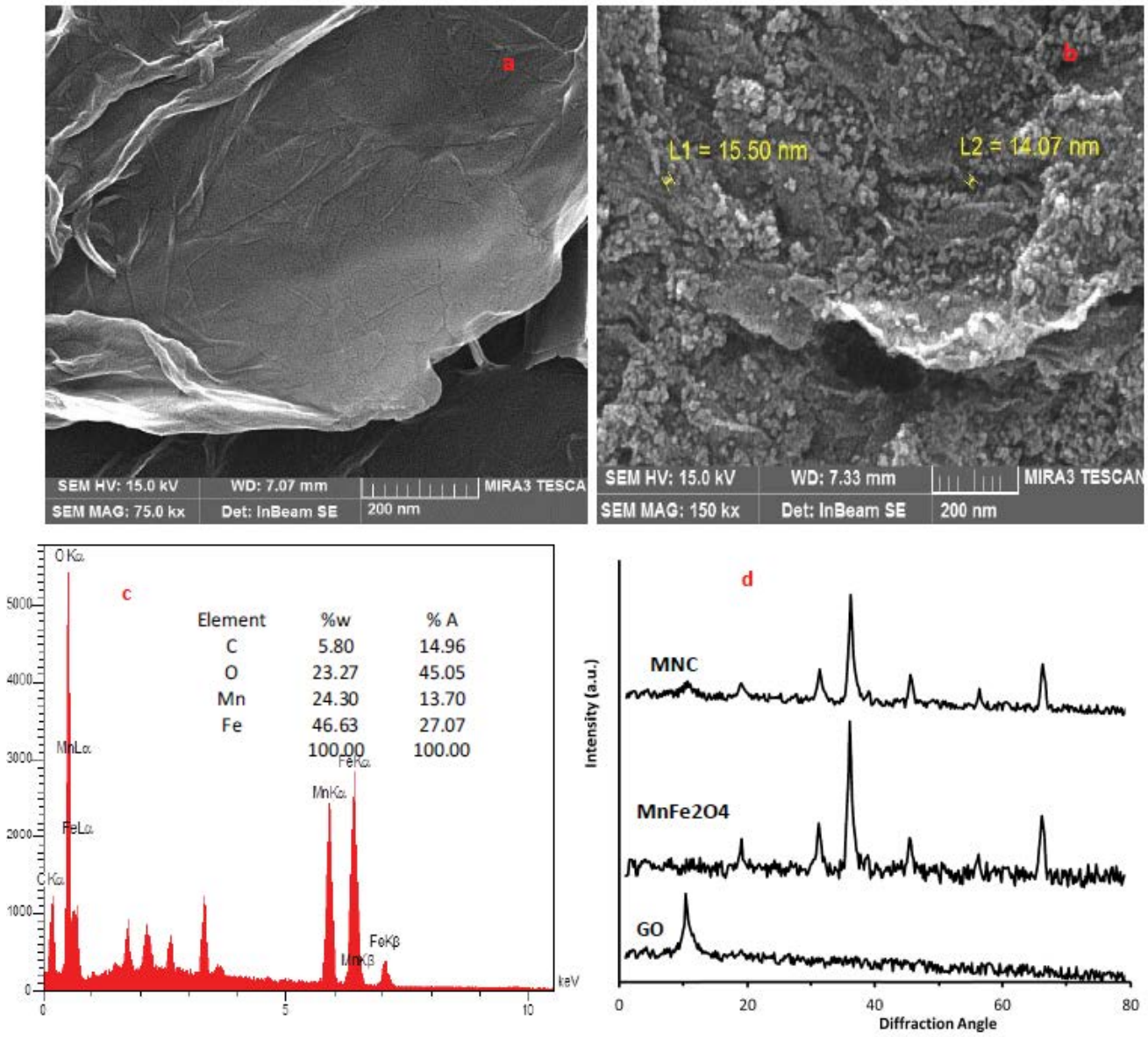

Fig. 1. SEM of GO (a) and MNC (b), (c) EDS of MNC and (d) XRD patterns of GO, $MnFe_2O_4$ and MNC.

magnetic confirmed the magnetism of the synthesized MNC. Thermogravimetric analysis (TGA) was measured with a Thermal Analyzer (METTLER TOLEDO System, TGA/SDTA 851) under a nitrogen atmosphere (flow rate 30 mL/min) at a heating rate of 10 to 950°C min^{-1}. TGA curves of $MnFe_2O_4$ and $MnFe_2O_4$-GO have been shown in Fig. 2b and the corresponding derivative thermogravimetry (DTG) plot of $MnFe_2O_4$-GO has been revealed in the inset of Fig. 2b. A slight weight loss around 90°C could be attributed to the vaporization of water molecules adsorbed on the materials. It was observed that $MnFe_2O_4$ is thermal stable but 11% weight loss at the temperature of 317°C for $MnFe_2O_4$-GO has approved the decomposition of labile functional groups on GO such as hydroxyl, carbonyl, carboxyl and epoxy.

FT-IR spectra of GO and $MnFe_2O_4$-GO were measured with a Fourier transform infrared spectroscopy (Rayleigh WQF-510A, Beijing, China) and the results have been illustrated in Fig. 2c. The absorption peaks at 1,050; 1,053 and 1,221 cm^{-1} correspond to the C–O stretching vibration of epoxy and alkoxy. The adsorption bands at 1,605 and 1,729 cm^{-1} represent the C=O and C=C stretching vibration, respectively. The two peaks around 2,885 cm^{-1} correspond to the asymmetric and symmetric vibration of C–H. The peaks at 3,400 and 3,410 cm^{-1} can be attributed to the O–H stretching vibration of carboxyl groups and the adsorbed water molecules. The characteristic band at 549 cm^{-1} which was observed just in $MnFe_2O_4$-GO FT-IR spectrum is assigned to intrinsic vibration of manganese ferrite and demonstrated that $MnFe_2O_4$ is present and supported on GO in $MnFe_2O_4$-GO.

The specific surface areas of $MnFe_2O_4$-GO were determined using nitrogen adsorption–desorption isotherms

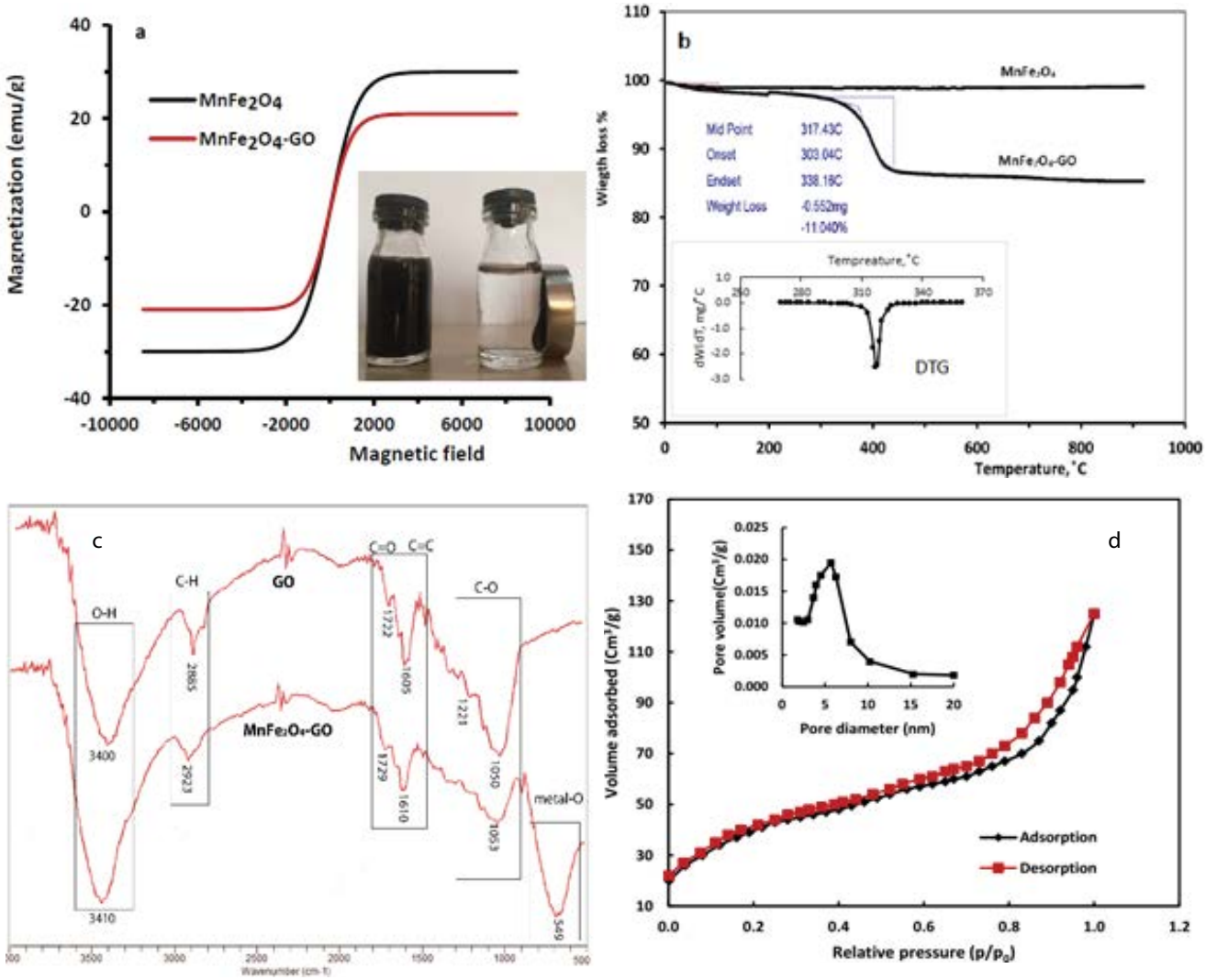

Fig. 2. (a) VSM and (b) TGA and DTG (inset) curves of $MnFe_2O_4$ and $MnFe_2O_4$-GO in nitrogen atmosphere, (c) FT-IR spectra of GO and $MnFe_2O_4$-GO and (d) N_2 adsorption–desorption isotherm of $MnFe_2O_4$-GO.

according to the Brunauer–Emmett–Teller (BET) method. BET adsorption experiments were carried out with Microtrac BELSORP-mini II at 77 K. Fig. 2d displays type IV adsorption–desorption isotherm, which revealed the mesoporous nature of adsorbent. The corresponding pore size distribution curve of $MnFe_2O_4$-GO has been shown in the inset of Fig. 2d that indicates most of the pores sizes are less than 20 nm with a central value of 6.8 nm. The specific surface area of $MnFe_2O_4$-GO was calculated as 108.6 $cm^2\ g^{-1}$.

3.2. Effect of pH and adsorbent dosage on the adsorption process

The potential of hydrogen (pH) is one of the most important parameters in adsorption processes as it affects the properties of the adsorbent's surface, ionization or dissociation of the adsorbate and eventually, the interaction between the adsorbent and adsorbate. GO nano-sheets have a negative surface charge in water solution due to ionization of phenolic and carboxylic groups that present on the GO sheets. The metal ions are present in the species of M^{2+}, $M(OH)^+$, $M(OH)_2$, depending on the pH of the aqueous solution. The precipitation constant of $Ni(OH)_2$ and $Co(OH)_2$ are 2.5×10^{-16} and 5.48×10^{-16}, then the precipitation pH of metal ions in the experimental conditions are around 7.8 and 7.7, respectively. In this study, the effect of pH on the adsorption of organic or inorganic contaminants was investigated in the pH range of 4–8 (Fig. 3). As can be observed, the adsorption capacities increase with an increasing pH value of the medium. The surface of MNC at low pH will be covered with H^+ ions which repulse strongly other positive charge ions for adsorption sites. With an increase in pH, the concentration of hydrogen ions in the solution decreases which leads to a decrease of positive surface charge and increases the adsorption of adsorbates by the adsorbent. The experimental results indicated that the pH of the initial dyestuff solution did not possess sharp influence on the adsorption of MB or TB. The nearly constant adsorption capacity of MB and TB over the pH range 5–8 (pH solution > $pK_{a,MB} = 3.8$, $pK_{a,TB} = 2.4$, 11.6) could be attributed to that the adsorption of dyestuffs on the MNC depends on both the electrostatic interaction and

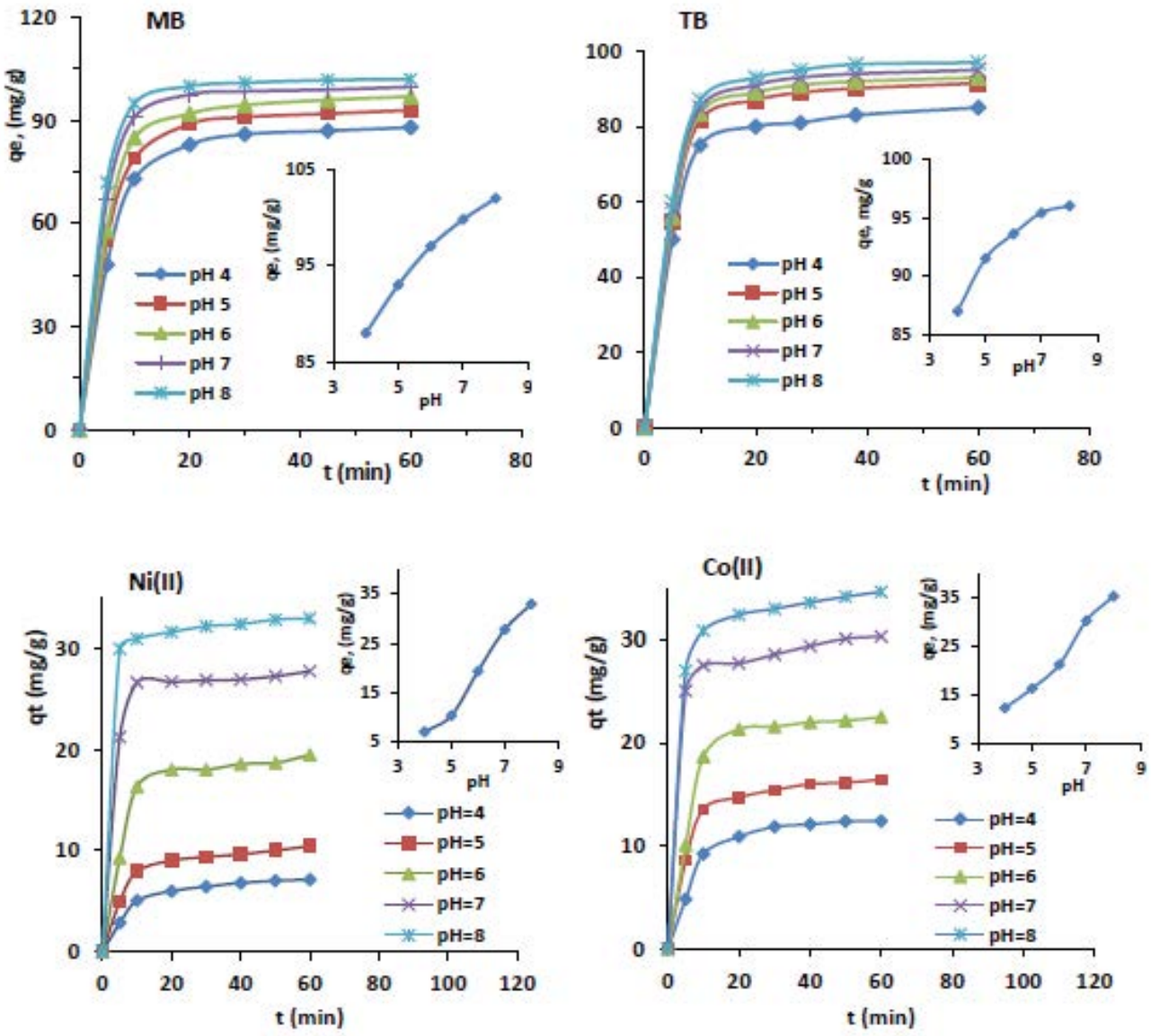

Fig. 3. Effect of pH on the adsorption capacities of dyestuffs (MB, TB) and metal ions (Co(II), Ni(II)) on MNC. Experimental conditions: sorbent dosage: 0.8 g L^{-1}, pollution concentration: 30 mg L^{-1}.

non-electrostatic such as hydrophobic interaction, Van der Waals forces, π–π interaction and hydrogen bonding in this system [31]. Therefore, pH 7.0 was selected as optimum pH for both organic and inorganic pollutants sorption, which is close to the natural pH of dyestuffs solution, as well as drinking water and there are no hydroxide precipitations of metal ions and the adsorption capacities are acceptable.

The effect of variation of adsorbent dosage from 0.4 to 1.1 g L^{-1} on the removal of pollutants was investigated in the separated solutions with the initial pollutant concentration 30 mg L^{-1}, pH 7.0 and contact time 30 min. The results have been shown in Fig. 4. As shown, the pollutant concentration in the solution decreases with increasing sorbent amount up to 0.8 g L^{-1} and after that, the curve was level off for all kind of pollutants. These results could be explained on the basis of a higher amount of the adsorbent provides greater surface area for a fixed initial solute concentration. Therefore 0.8 g L^{-1} was selected as an optimum adsorbent dosage for more studies.

3.3. Adsorption kinetics

As observed in Fig. 3, the adsorption process of pollutants on $MnFe_2O_4$-GO was very quick such that 90% of the equilibrium adsorption was completed in the first 10 min and the final equilibrium was achieved within 20 min under our experimental conditions. In order to predict the sorption kinetics of pollutants on the MNC, two common adsorption kinetic models were employed: pseudo-first-order (Eq. (2)) and pseudo-second-order (Eq. (3)). The results of this study have been shown in Figs. 5 and 6 and the kinetic parameters drawn from the figures are summarized in Table 1. As shown, the pseudo-first-order model with very low determination

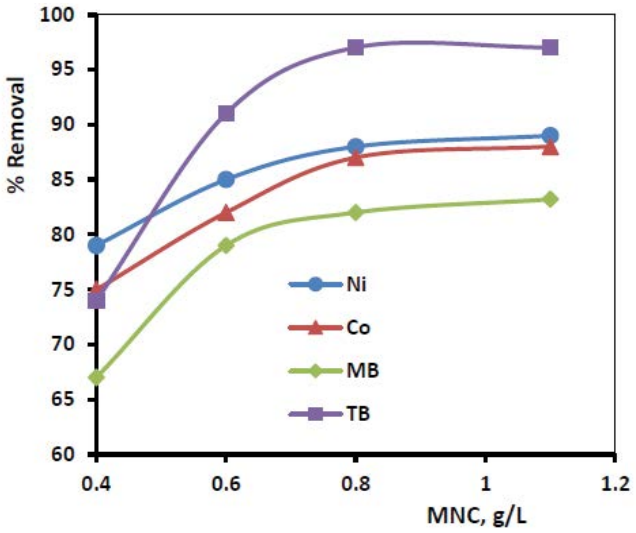

Fig. 4. Effect of adsorbent dosage on the removal efficiency of pollutant. Experimental conditions: pollution concentration 30 mg L^{-1}, pH 7.0, contact time 30 min, sorbent dosage: 0.4, 0.6, 0.8 and 1.1 g L^{-1}.

coefficients might not be suitable to describe the adsorption process, while the pseudo-second-order equation fits well to the experimental data with determination coefficients higher than 0.99. The pseudo-second-order equation is based on the assumption that the rate limiting step might be chemical adsorption between sorbent and sorbate. In comparison with the adsorption equilibrium time of other adsorbents (Table 3), the MNC has shown remarkable rapid adsorption kinetics, which makes it a suitable adsorbent for practical applications.

3.4. Adsorption isotherms

The equilibrium data of both organic and inorganic contaminates adsorption on MNC were modelled using the Langmuir (Eq. (4)) and Freundlich equations (Eq. (5)). The results have been shown in Figs. 7 and 8. The results drawn from these figures indicated that both of the adsorbates (organic and inorganic pollutants) can be well fitted by the Langmuir model ($R^2 > 0.99$), indicating that metal ions and dye molecules are adsorbed onto MNC by the mean of the monolayer, not multilayer adsorption. The Langmuir model assumes that there are the identical energy sites on the

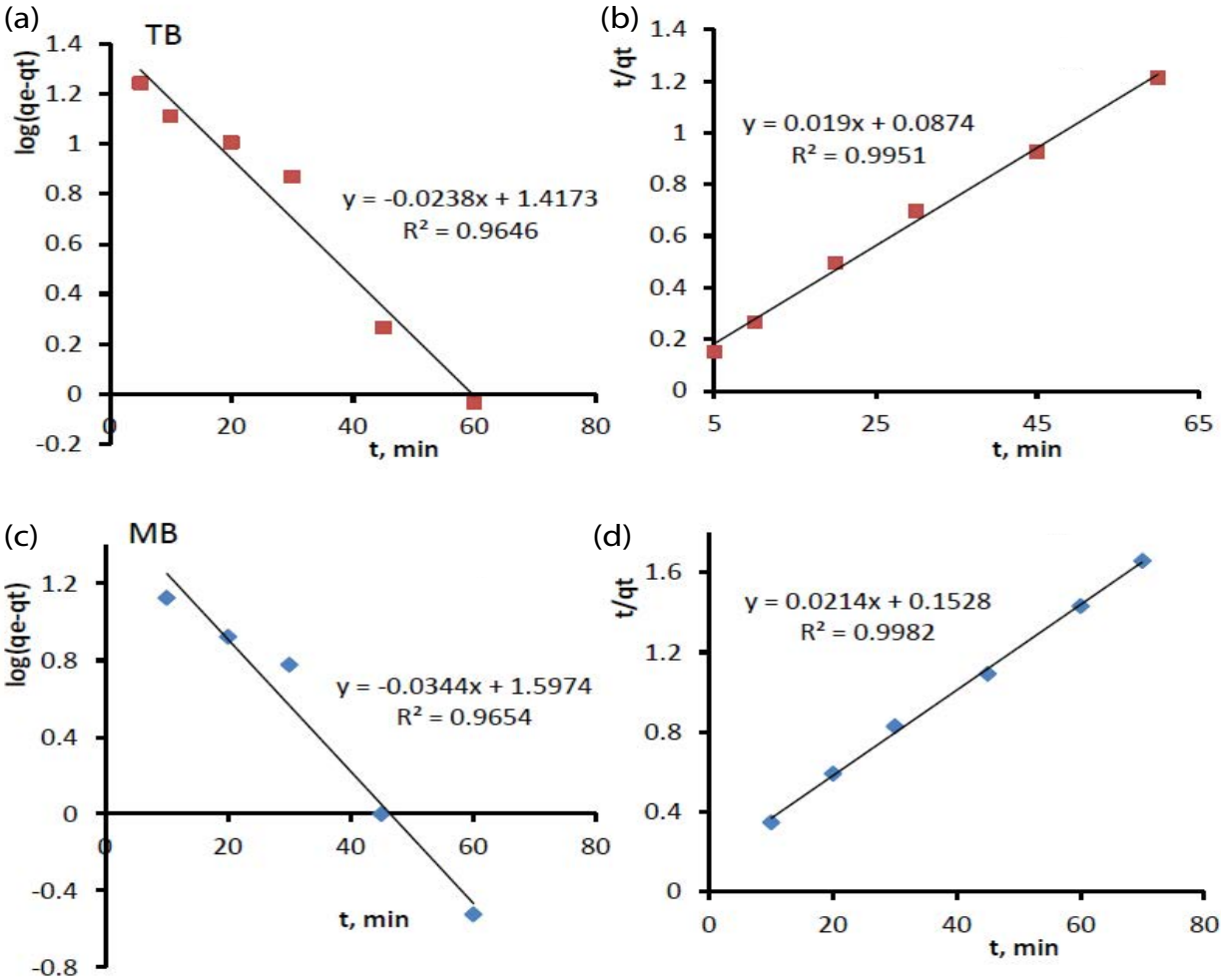

Fig. 5. Kinetic models for adsorption of dyes on MNC ((a) and (c)) pseudo-first-order and ((b) and (d)) pseudo-second-order. Experimental conditions: sorbent dosage: 0.8 g L^{-1}, initial pollutant concentration: 30 mg L^{-1}, pH: 7.0.

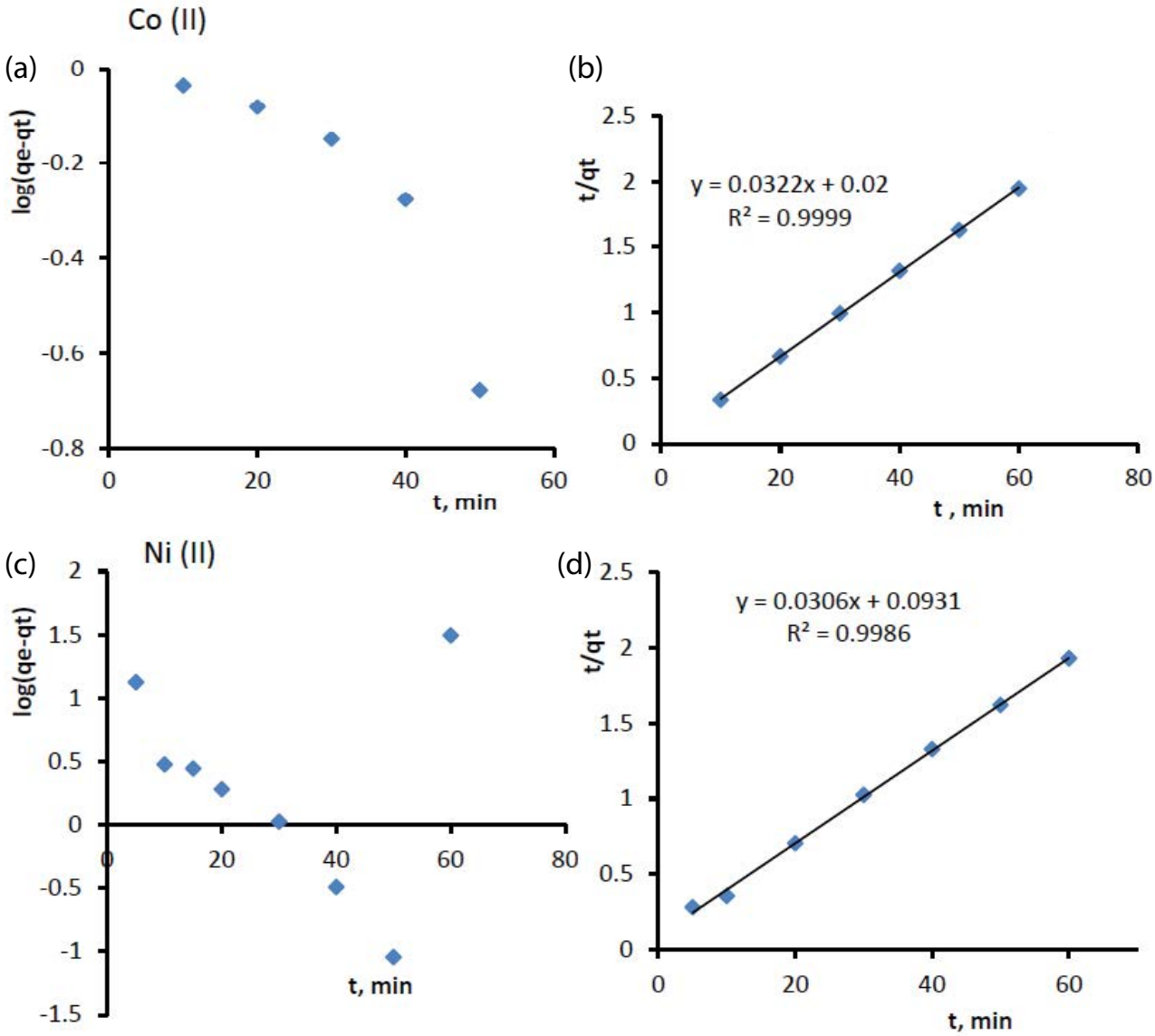

Fig. 6. Kinetic models for adsorption of metal ions ((a) and (c)) pseudo-first-order and ((b) and (d)) pseudo-second-order models. Experimental conditions: sorbent dosage: 0.8 g L^{-1}, the initial pollutant concentration: 30 mg L^{-1}, pH: 7.0.

adsorbent surface and that adsorbate is located at a single site. In other words, it predicts the formation of a monolayer of the adsorbate on the adsorbent surface, whereas the Freundlich model is an empirical equation employed to describe equilibrium on heterogeneous surfaces and hence does not assume monolayer capacity. The Langmuir parameters including determination coefficient, the maximum capacity of the sorbent (q_m), the energy of adsorption (b) and Freundlich parameters including adsorption capacity (K_f) and adsorption intensity (n) have been calculated and the results are summarized in Table 2.

A literature review of the adsorption capacities of the different kinds of graphene-based magnetic nano-sorbent for removal of Co(II), Ni(II) MB and TB have been summarized in Table 3 and compared with MNC. Comparison of our results with what has been presented in Table 3 confirmed that the adsorption capacities of the MNC towards Co(II), Ni(II), MB and TB were comparable with other excellent adsorbents, and in some cases, they excelled.

3.4. Adsorption thermodynamics

The effect of temperature on the adsorption process was studied at three different temperatures: 298, 313 and 333 K with initial pH 7.0, sorbent dose 0.8 g L^{-1} and initial concentration of metal ions or dyes 30 mg L^{-1}. Gibbs free energy change was calculated by the following equation [30]:

$$\Delta G^{\circ} = -RT\ln b \tag{6}$$

where $\Delta G°$ is the standard free energy change (J mol^{-1}), R gas universal constant (8.314 J mol^{-1} K^{-1}), T absolute temperature (K) and b Langmuir constant.

Table 1
Kinetics parameters for the adsorption 10, 20, 30 mg L^{-1} of metal ions or dyestuffs on the MNC at 25°C

Pollutant		First order			Second order		
		k_1	q_e (mg g^{-1})	R^2	k_2	q_e (mg g^{-1})	R^2
TB	10	5.431×10^{-3}	26.13	0.9654	1.102×10^{-3}	52.67	0.9951
	20	5.012×10^{-3}	55.74	0.9659	2.101×10^{-3}	81.92	0.9924
	30	7.732×10^{-3}	96.22	0.9646	1.212×10^{-3}	108.96	0.9951
MB	10	7.925×10^{-3}	39.53	0.9654	6.102×10^{-3}	46.32	0.9982
	20	9.300×10^{-3}	83.77	0.9757	3.221×10^{-3}	96.73	0.9995
	30	7.801×10^{-3}	92.53	0.9654	1.112×10^{-3}	119.87	0.9982
Co(II)	10	0.067	1.49	0.6502	0.064	10.47	0.9987
	20	0.052	1.87	0.6767	0.072	18.93	0.9998
	30	0.054	1.58	0.8150	0.024	31.25	0.9999
Ni(II)	10	0.073	4.24	0.9234	0.031	12.82	0.9993
	20	0.098	12.30	0.9262	0.015	32.68	0.9986
	30	0.097	13.74	0.9559	0.010	42.62	0.9992

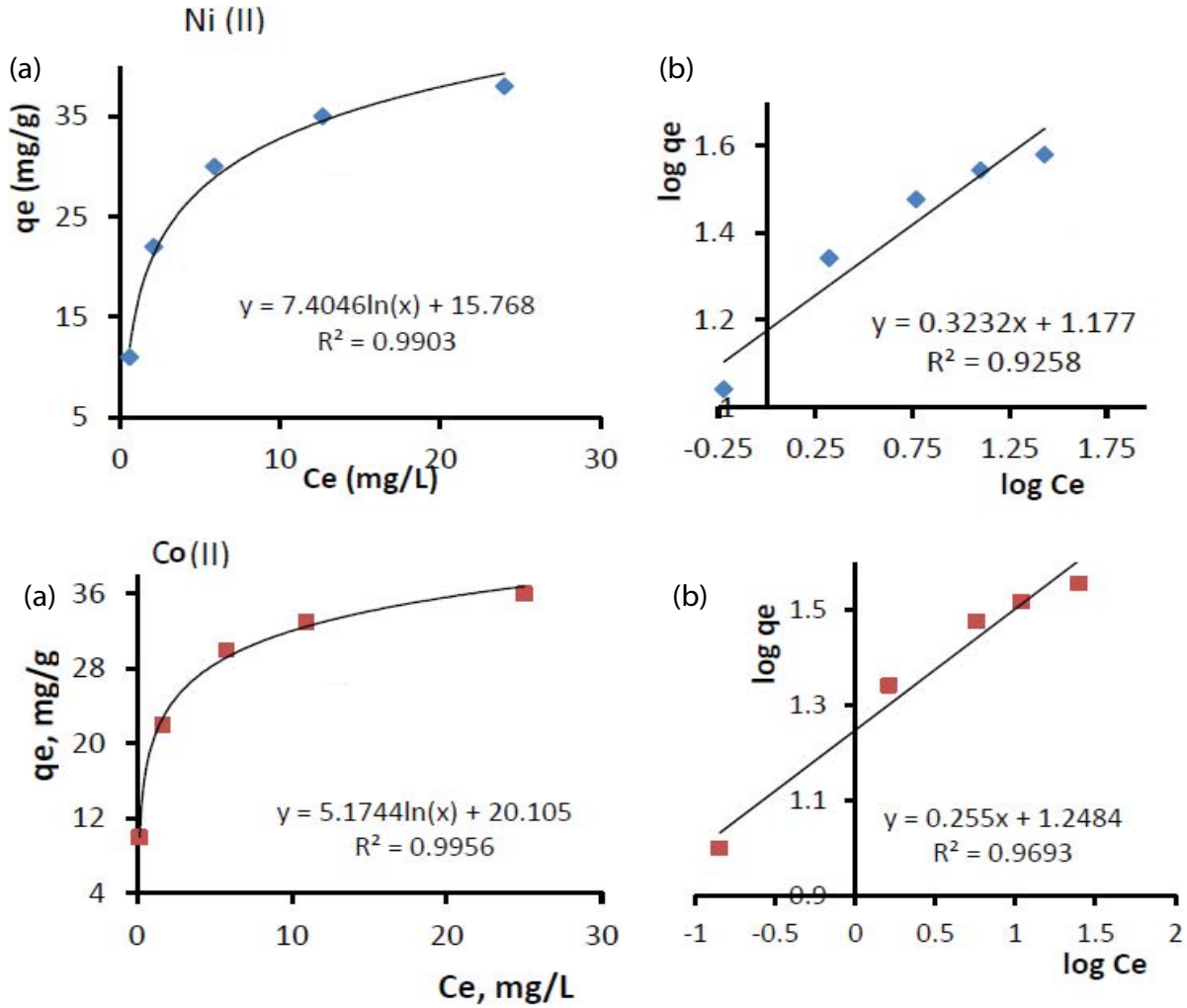

Fig. 7. Adsorption isotherms of metal ions: (a) Langmuir and (b) linearized Freundlich model. Experimental conditions: sorbent dosage: 0.8 g L^{-1}, contact time: 20 min, the initial pollutant concentration: 10, 30, 50, 70, 100 mg L^{-1}, pH: 7.0.

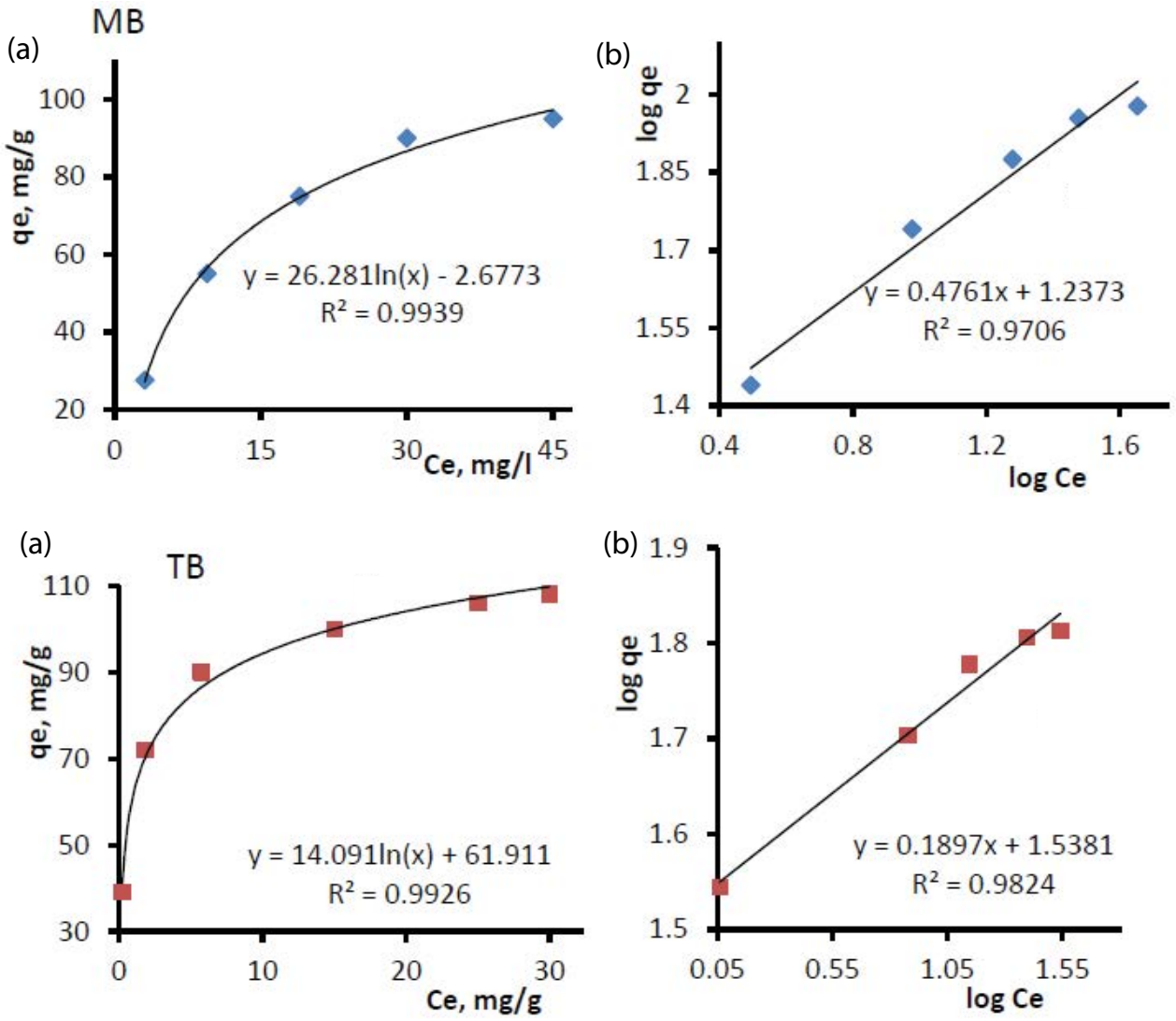

Fig. 8. Adsorption isotherms of dyestuffs: (a) Langmuir and (b) linearized Freundlich model. Experimental conditions: sorbent dosage: 0.8 g L^{-1}, contact time: 20 min, initial pollutant concentration: 10, 30, 50, 70, 100 mg L^{-1}, pH: 7.0.

Table 2
Isotherm parameters for the adsorption of metal ions and dyestuffs onto the MNC

Pollutant	Langmuir model			Freundlich model		
	q_m (mg g^{-1})	b (L mg^{-1})	R^2	n	K_f (mg g^{-1})(L mg^{-1})$^{1/n}$	R^2
Ni(II)	46.71 ± 1.6	0.38 ± 0.01	0.9935	3.09 ± 0.11	15.03 ± 0.57	0.9258
Co(II)	37.02 ± 1.7	1.01 ± 0.03	0.9983	3.92 ± 0.16	17.70 ± 0.71	0.9693
MB	125.03 ± 4.3	0.09 ± 0.03	0.9983	2.12 ± 0.09	17.37 ± 0.76	0.9706
TB	110.01 ± 4.6	1.05 ± 0.04	0.9989	5.27 ± 0.20	34.51 ± 1.36	0.9824

±Standard deviation for three replicates.

Other thermodynamic parameters $\Delta H°$ (enthalpy change) and $\Delta S°$ (entropy change) can be estimated by the following equation:

$$\Delta G^\circ = \Delta H^\circ - T\Delta S^\circ \quad (7)$$

The calculated thermodynamic parameters for the adsorption of pollutants onto the MNC are given in Table 4. The negative values of $\Delta G°$ indicate that the adsorption processes are spontaneous for both organic and inorganic pollutants at room temperature. More negative

Table 3
List of the adsorption capacities has been reported for the removal of nickel, cobalt and Methylene blue using various magnetic graphene-based adsorbents

Adsorbent	q_e (mg g^{-1})				Equilibrium time	Reference
	Ni(II)	Co(II)	MB	TB		
Fe_3O_4-RGO[a]	74.6	–	–	–	24 h	[27]
Fe_3O_4-GO	156.0	–	–	–	24 h	[32]
SDS-GO[b]	55.2	–	–	–	24 h	[33]
Graphene/delta-MnO_2	46.6	–	–	–	120 min	[34]
Fe-Mn oxide RGO[c]	228.0	–	–	–	150 min	[35]
Fe_3O_4-GO	–	13.0	–	–	24 h	[36]
β-CD-GO[d]	–	72.4	–	–	24 h	[37]
Amination GO	–	116.4	–	–	24 h	[38]
GO-APTS-poly(AMPScoMA)	–	238.4	416.0	–	6 h	[39]
β-CDC-GO[e]	–	–	84.3	–	80 min	[40]
RGO–$MnFe_2O_4$	–	–	34.7	–	5 min	[41]
Fe_3O_4 -GO	–	–	306.5	–	250 min	[42]
Pt/Rh -GO	–	–	346.8	–	40 min	[43]
Fe_3O_4-GO	–	–	96.1	–	12 h	[44]
$MnFe_2O_4$-GO	46.7	37.0	125.0	110.0	20 min	This work

[a]Reduced graphene oxide.
[b]Sodium dodecyl sulfate–functionalized graphene oxide.
[c]Iron–manganese binary oxide reduced graphene oxide.
[d]Beta-cyclodextrin modified graphene oxide.
[e]Beta-cyclodextrin chitosan graphene oxide.

Table 4
Values of thermodynamic parameters for the sorption of organic and inorganic pollutant

Pollutant	$\Delta H°$ (kJ mol^{-1})	$\Delta S°$ (J mol^{-1} K)	$-\Delta G°$ (kJ mol^{-1})		
			298 K	313 K	333 K
Co(II)	118.7	491.5	27.2	35.2	45.0
Ni(II)	46.8	242.8	25.1	29.2	34.0
MB	94.8	412.4	25.4	31.3	39.8
TB	111.5	477.6	31.1	37.4	47.8

values of $\Delta G°$ with increasing temperature demonstrate that degree of feasibility and spontaneity of adsorption increases at higher temperature. The positive values of $\Delta H°$ and $\Delta S°$ indicate the endothermic nature of the adsorption process and the increased disorder at the solid–solution interface during the adsorption, respectively.

3.5. Recovery of MNC

To determine the recoverability of the magnetic nano-adsorbent, five cycles of consecutive adsorption–desorption experiments were performed according to the protocols mentioned in section 2.3.5. The adsorption capacities were calculated for each cycle by using Eq. (1). The results are shown in Fig. 9. As can be seen, no significant decrease in the adsorption capacities was observed. These results showed that $MnFe_2O_4$-GO composite could be an efficient and cost-effective adsorbent for metal ions and cationic dyes due to the excellent reusability performance.

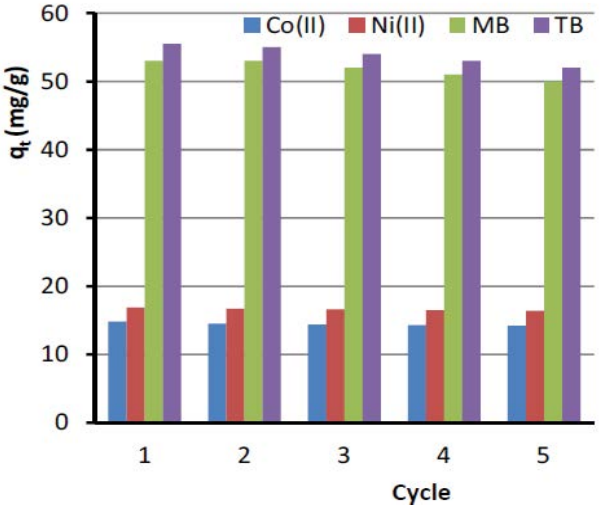

Fig. 9. Recoverability of MNC for adsorption of metal ions and dyes during five cycles. Experimental conditions: sorbent dosage: 0.8 g L^{-1}, initial pollutant concentration: 15 mg L^{-1}, pH: 7.0, contact time: 20 min.

3.6. Adsorption study in organic/inorganic multiple systems

Adsorption experiments in binary systems were carried out to investigate the competitive sorption between

Table 5
Adsorption capacities of MNC for removal of pollutant in multiple systems

	Co(II) (mg L^{-1})	Ni(II) (mg L^{-1})	TB (mg L^{-1})	MB (mg L^{-1})	q_e (mg g^{-1})
Co(II)	30	–	–	–	29.2
	30	–	–	30	37.5
	30	–	30	–	44.3
	30	–	30	30	43.6
Ni(II)	–	30	–	–	31.9
	–	30	–	30	38.8
	–	30	30	–	39.3
	–	30	30	30	37.1
TB	–	–	30	–	94.8
	30	–	30	–	95.2
	–	30	30	–	94.1
	–	–	30	30	85.4
MB	–	–	–	30	101.8
	–	30	–	30	102.1
	30	–	–	30	99.8
	–	–	30	30	88.2

two kinds of pollutants on MNC. The concentration of each pollutant in a binary system was the same as 30 mg L^{-1}, pH 7.0 and nano-adsorbent 0.8 g L^{-1} and q_t was calculated after 20 min. The results were very interesting. The maximum adsorption capacities of organic pollutant were almost the same in the presence or absence of inorganic pollutant and there were no any significant differences between them but, that for inorganic pollutants have been changed and increased in the presence of dyestuff. The results have been summarized in Table 5. As can be seen, q_e of cobalt in single medium was 29.2 (mg g^{-1}) but in presence of 30 mg L^{-1} of MB increased to 37.5 (mg g^{-1}) and in presence of 30 mg L^{-1} of TB increased to 44.3 (mg g^{-1}), even in presence of both colour q_e was calculated as 43.6 (mg g^{-1}) which was higher than that in absence of dyestuff. Since the results of spectrophotometric analysis did not show any evidence of complex formation between inorganic ions and dyestuffs, these results could be attributed to this fact that covering of MNC surface with dye molecules increase surface functional groups of nano-sorbent consequently increases the sorption capacity for removal of metal ions by MNC.

The MNC was also used for purification of a water solution containing multiple pollutants simultaneously. The concentrations of all pollutants were the same at 30 mg L^{-1} and adsorbent dose 0.8 g L^{-1}. As expected according to the results obtained in binary systems, other coexisting ions did not affect the adsorption capacities of MNC for metal ions significantly, but the adsorption capacity of organic compound decreased from 94.8 to 85.4 mg g^{-1} for TB and from 101.8 to 88.2 mg g^{-1} for MB. It was estimated that this reduction was due to the saturation of the adsorbent surface, therefore, the adsorbent dose has been increased from 0.8 to 1.2 g L^{-1} and the experiment was repeated again. The results showed that the adsorptive removal of organic compound increased with increasing of the adsorbent dose and the same removal efficiency was achieved again for the organic pollutant. In summary, MNC could be introduced as a high-performance adsorbent for simultaneous and fast removal of multiple pollutants.

4. Conclusion

In this study, $MnFe_2O_4$-graphene oxide nano-composite (MNC) was synthesized and characterized by SEM, EDS and XRD techniques. The results were presented that graphene nano-sheets decorated with $MnFe_2O_4$ nanoparticles with an average diameter of less than 20 nm have been synthesized. The MNC showed potential power for adsorption removal of organic (MB and TB) and inorganic (Co and Ni) contaminants separately and simultaneously. At the end of each experiment, nanoparticles along with the contaminants could be collected and removed by using an external magnet, easily. Batch experiments were carried out to quantify the adsorption isotherms and kinetics of MNC in the removal of inorganic and organic pollutants at 25°C. The results showed the Langmuir isotherm and pseudo-second-order kinetic model could well interpret the adsorption process. The thermodynamic results showed that the adsorption process was spontaneous and endothermic. The regeneration ability of MNC for continuous use in a straightforward way was investigated and the results showed that MNC could introduce a very promising multifunctional water purifier with high performance and reusability for water purification.

Acknowledgement

The authors wish to express their gratitude to the Shahid Beheshti University of Medical Sciences Research Council for the support of this work.

References

[1] WHO Fact sheet, Available at http://www.who.int/mediacentre/factsheets/fs391/en/November 2016.
[2] S.S. Khaloo, M. Torabbeigi, R.K. Jazani, M. Douraghi, Z. Ghalavand, Laboratory waste minimization by recovery of silver as nano-silver colloidal dispersion from waste silver chloride, J. Mater. Cycles Waste Manage., 15 (2013) 342–347.
[3] M.S. Melchiors, M. Piovesan, V.R. Becegato, V.A. Becegato, E.B. Tambourgi, A.T. Paulino, Treatment of wastewater from the dairy industry using electroflocculation and solid whey recovery, J. Environ. Manage., 182 (2016) 574–580.
[4] S. Chong, G. Zhang, H. Tian, H. Zhao, Rapid degradation of dyes in water by magnetic Fe^0/Fe_3O_4/graphene composites, J. Environ. Sci., 44 (2016) 148–157.
[5] G. Safari, M. Hosseini, M. Seyed-Salehi, H. Kamani, J. Jaafari, A. Mahvi, Photocatalytic degradation of tetracycline using nanosized titanium dioxide in aqueous solution, Int. J. Environ. Sci. Technol., 12 (2015) 603–616.
[6] A. Dalvand, R. Nabizadeh, M. Reza Ganjali, M. Khoobi, S. Nazmara, A. Hossein Mahvi, Modeling of Reactive Blue 19 azo dye removal from colored textile wastewater using L-arginine-functionalized Fe_3O_4 nanoparticles: Optimization, reusability, kinetic and equilibrium studies, J. Magn. Magn. Mater., 404 (2016) 179–189.
[7] M. Shirmardi, A.H. Mahvi, B. Hashemzadeh, A. Naeimabadi, G. Hassani, M.V. Niri, The adsorption of malachite green (MG) as a cationic dye onto functionalized multi walled carbon nanotubes, Korean J. Chem. Eng., 30 (2013) 1603–1608.

[8] A. Takdastan, A.H. Mahvi, E.C. Lima, M. Shirmardi, A.A. Babaei, G. Goudarzi, A. Neisi, M. Heidari Farsani, M. Vosoughi, Preparation, characterization, and application of activated carbon from low-cost material for the adsorption of tetracycline antibiotic from aqueous solutions, Water Sci. Technol., 74 (2016) 2349–2363.
[9] M. Shirmardi, A.H. Mahvi, A. Mesdaghinia, S. Nasseri, R. Nabizadeh, Adsorption of acid red18 dye from aqueous solution using single-wall carbon nanotubes: kinetic and equilibrium, Desal. Wat. Treat., 51 (2013) 6507–6516.
[10] J.G. Yu, L.Y. Yu, H. Yang, Q. Liu, X.H. Chen, X.Y. Jiang, X.Q. Chen, F.P. Jiao, Graphene nanosheets as novel adsorbents in adsorption, preconcentration and removal of gases, organic compounds and metal ions, Sci. Total Environ., 502 (2015) 70–79.
[11] N. Xiao, D. Lau, W. Shi, J. Zhu, X. Dong, H.H. Huang, Q. Yan, A simple process to prepare nitrogen-modified few-layer graphene for a supercapacitor electrode, Carbon, 57 (2013) 184–190.
[12] S. Benítez-Martínez, M. Valcárcel, Graphene quantum dots in analytical science, TrAC, Trends Anal. Chem., 72 (2015) 93–113.
[13] F. Liu, Y. Piao, J.S. Choi, T.S. Seo, Three-dimensional graphene micropillar based electrochemical sensor for phenol detection, Biosens. Bioelectron., 50 (2013) 387–392.
[14] E. Song, D. Cheng, Y. Song, M. Jiang, J. Yu, Y. Wang, A graphene oxide-based FRET sensor for rapid and sensitive detection of matrix metalloproteinase 2 in a human serum sample, Biosens. Bioelectron., 47 (2013) 445–450.
[15] M. Li, W. Xu, W. Wang, Y. Liu, B. Cui, X. Guo, Facile synthesis of specific FeMnO3 hollow sphere/graphene composites and their superior electrochemical energy storage performances for supercapacitor, J. Power Sources, 248 (2014) 465–473.
[16] H. Zhou, G. Han, D. Fu, Y. Chang, Y. Xiao, H.-J. Zhai, Petal-shaped poly(3,4-ethylenedioxythiophene)/sodium dodecyl sulfate-graphene oxide intercalation composites for high-performance electrochemical energy storage, J. Power Sources, 272 (2014) 203–210.
[17] A.A. Ensafi, M. Jafari-Asl, B. Rezaei, A new strategy for the synthesis of 3-D Pt nanoparticles on reduced graphene oxide through surface functionalization, Application for methanol oxidation and oxygen reduction, Electrochim. Acta, 130 (2014) 397–405.
[18] S. Yang, G. Wang, G. Li, J. Du, L. Qu, Decoration of graphene modified carbon paste electrode with flower-globular terbium hexacyanoferrate for nanomolar detection of rutin, Electrochim. Acta, 144 (2014) 268–274.
[19] M.G. Kochameshki, A. Marjani, M. Mahmoudian, K. Farhadi, Grafting of diallyldimethylammonium chloride on graphene oxide by RAFT polymerization for modification of nanocomposite polysulfone membranes using in water treatment, Chem. Eng. J., 309 (2017) 206–221.
[20] S.H. Ryu, A.M. Shanmugharaj, Influence of long-chain alkylamine-modified graphene oxide on the crystallization, mechanical and electrical properties of isotactic polypropylene nanocomposites, Chem. Eng. J., 244 (2014) 552–560.
[21] L.Z. Liu, S.B. Tian, Y.Z. Long, W.X. Li, H.F. Yang, J.J. Li, C.Z. Gu, Tunable periodic graphene antidot lattices fabricated by e-beam lithography and oxygen ion etching, Vacuum, 105 (2014) 21–25.
[22] L. Liu, X. Yue, J. Zhao, Q. Cheng, J. Tang, Graphene antidot lattices as potential electrode materials for supercapacitors, Physica E Low-dimens. Syst. Nanostruct., 69 (2015) 316–321.
[23] S.S. Khaloo, M.A. Marzaleh, M. Kavousian, S.B. Gendeshmin, Graphene oxide coated wad as a new sorbent in fixed bed column for the removal of crystal violet from contaminated water, Sep. Sci. Technol., 51 (2016) 1–10.
[24] T. Qi, C. Huang, S. Yan, X.-J. Li, S.-Y. Pan, Synthesis, characterization and adsorption properties of magnetite/reduced graphene oxide nanocomposites, Talanta, 144 (2015) 1116–1124.
[25] K. Ouyang, C. Zhu, Y. Zhao, L. Wang, S. Xie, Q. Wang, Adsorption mechanism of magnetically separable Fe_3O_4/graphene oxide hybrids, Appl. Surf. Sci., 355 (2015) 562–569.
[26] P.J. Robinson, P. Dunnill, M.D. Lilly, The properties of magnetic supports in relation to immobilized enzyme reactors, Biotechnol. Bioeng., 15 (1973) 603–606.
[27] N.T.V. Hoan, N.T.A. Thu, H.V. Duc, N.D. Cuong, D.Q. Khieu, V. Vo, Fe_3O_4/reduced graphene oxide nanocomposite: synthesis and its application for toxic metal ion removal, J. Chem., 2016 (2016) 10.
[28] S.E. Moradi, Highly efficient removal of amoxicillin from water by magnetic graphene oxide adsorbent, Chem. Bull. Politehnica Univ. (Timisoara), 60 (2015) 41–48.
[29] H. Ting, K. Lingyu, G. Xiaoyu, W. Yiping, W. Feng, W. Ying, Y. Haifeng, Magnetic ferrous-doped graphene for improving Cr(VI) removal, Mater. Res. Express, 3 (2016) 045006.
[30] S.S. Khaloo, A.H. Matin, S. Sharifi, M. Fadaeinia, N. Kazempour, S. Mirzadeh, Equilibrium, kinetic and thermodynamic studies of mercury adsorption on almond shell, Water Sci. Technol., 65 (2012) 1341–1349.
[31] A.A. Babaei, E.C. Lima, A. Takdastan, N. Alavi, G. Goudarzi, M. Vosoughi, G. Hassani, M. Shirmardi, Removal of tetracycline antibiotic from contaminated water media by multi-walled carbon nanotubes: operational variables, kinetics, and equilibrium studies, Water Sci. Technol., 74 (2016) 1202–1216.
[32] G. Lujaniene, S. Semcuk, A. Lecinskyte, I. Kulakauskaite, K. Mazeika, D. Valiulis, V. Pakstas, M. Skapas, S. Tumenas, Magnetic graphene oxide based nano-composites for removal of radionuclides and metals from contaminated solutions, J. Environ. Radio., 166 (2017) 166–174.
[33] E.C. Salihi, J.B. Wang, D.J.L. Coleman, L. Siller, Enhanced removal of nickel(II) ions from aqueous solutions by SDS-functionalized graphene oxide, Sep. Sci. Technol., 51 (2016) 1317–1327.
[34] Y.M. Ren, N. Yan, Q. Wen, Z.J. Fan, T. Wei, M.L. Zhang, J. Ma, Graphene/delta-MnO_2 composite as adsorbent for the removal of nickel ions from wastewater, Chem. Eng. J., 175 (2011) 1–7.
[35] D. Nandi, I. Saha, S.S. Ray, A. Maity, Development of a reduced-graphene-oxide based superparamagnetic nanocomposite for the removal of nickel (II) from an aqueous medium via a fluorescence sensor platform, J. Colloid Interface Sci., 454 (2015) 69–79.
[36] M.C. Liu, C.L. Chen, J. Hu, X.L. Wu, X.K. Wang, Synthesis of magnetite/graphene oxide composite and application for cobalt(II) removal, J. Phys. Chem. C, 115 (2011) 25234–25240.
[37] W.C. Song, J. Hu, Y. Zhao, D.D. Shao, J.X. Li, Efficient removal of cobalt from aqueous solution using beta-cyclodextrin modified graphene oxide, RSC Adv., 3 (2013) 9514–9521.
[38] F. Fang, L.T. Kong, J.R. Huang, S.B. Wu, K.S. Zhang, X.L. Wang, B. Sun, Z. Jin, J. Wang, X.J. Huang, J.H. Liu, Removal of cobalt ions from aqueous solution by an amination graphene oxide nanocomposite, J. Hazard. Mater., 270 (2014) 1–10.
[39] R. Sahraei, K. Hemmati, M. Ghaemy, Adsorptive removal of toxic metals and cationic dyes by magnetic adsorbent based on functionalized graphene oxide from water, RSC Adv., 6 (2016) 72487–72499.
[40] L.L. Fan, C.N. Luo, M. Sun, H.M. Qiu, X.J. Li, Synthesis of magnetic beta-cyclodextrin-chitosan/graphene oxide as nano-adsorbent and its application in dye adsorption and removal, Colloid. Surf. B-Biointerf., 103 (2013) 601–607.
[41] S. Bai, X.P. Shen, X. Zhong, Y. Liu, G.X. Zhu, X. Xu, K.M. Chen, One-pot solvothermal preparation of magnetic reduced graphene oxide-ferrite hybrids for organic dye removal, Carbon, 50 (2012) 2337–2346.
[42] Y.F. Guo, J. Deng, J.Y. Zhu, X.J. Zhou, R.B. Bai, Removal of mercury(II) and methylene blue from a wastewater environment with magnetic graphene oxide: adsorption kinetics, isotherms and mechanism, RSC Adv., 6 (2016) 82523–82536.
[43] Y. Yildiz, T.O. Okyay, B. Sen, B. Gezer, S. Kuzu, A. Savk, E. Demir, Z. Dasdelen, H. Sert, F. Sen, Highly monodisperse Pt/Rh nanoparticles confined in the graphene oxide for highly efficient and reusable sorbents for methylene blue removal from aqueous solutions, Chemistry Select, 2 (2017) 697–701.
[44] N.N. Liao, Z.S. Liu, W.J. Zhang, S.G. Gong, D.M. Ren, L.J. Ke, K. Lin, H. Yang, F. He, H.L. Jiang, Preparation of a novel Fe_3O_4/graphene oxide hybrid for adsorptive removal of methylene blue from water, J. Macromol. Sci. Part A Pure Appl. Chem., 53 (2016) 276–281.